1. Tomasz RYMARCZYK[1,2], 2. Grzegorz KŁOSOWSKI[3], 3. Mirosław GUZIK[1], 4. Konrad NIDERLA[1], 5. Jerzy LIPSKI[3]

University of Economics and Innovation in Lublin (1), Research and Development Center Netrix S.A. (2), Lublin University of Technology (3)

ORCID: 1. 0000-0002-3524-9151; 2. 0000-0001-7927-3674; 3. 0000-0003-3351-9039; 4. 0000-0003-1280-0622; 5. 0000-0002-2542-2950

doi:10.15199/48.2021.12.35

Hybrid machine learning in electrical impedance tomography

Abstract. *Artificial intelligence plays an increasingly important role in industrial tomography. In industry, various types of tomography can be used, where one of the criteria for classification may be a physical phenomenon. Thus, it is possible to distinguish computed tomography, impedance tomography, ultrasound tomography, capacitance tomography, radio-tomographic imaging, and others. The research described in this paper focuses on the EIT method used to imaging reactors' interior and industrial vessels. Inside the tested reactor, there may be a liquid of various densities containing solid inclusions or gas bubbles. The presented research presents the concept of transforming measurements into tomographic images using many known, homogeneous methods simultaneously. It is assumed that there is no single method of solving the inverse problem for all possible measurement cases. Depending on the specifics of the studied case, various methods generate reconstructions that differ in terms of accuracy and resolution. The presented research proves that the proposed approach justifies the increase in computational complexity, ensuring higher quality of tomographic images.*

Streszczenie. *W tomografii przemysłowej coraz większą rolę odgrywa sztuczna inteligencja. W przemyśle można stosować różne rodzaje tomografii, gdzie jednym z kryteriów podziału może być wykorzystywane zjawisko fizyczne. W ten sposób można wyróżnić tomografię komputerową, tomografię impedancyjną, tomografię ultradźwiękową, tomografię pojemnościową, obrazowanie radio-tomograficzne i inne. Opisywane w niniejszym opracowaniu badania skupiają się na metodzie EIT Wykorzystywanej do obrazowania wnętrza reaktorów i zbiorników przemysłowych. Wewnątrz badanego reaktora może znajdować się ciecz o różnej gęstości, zawierająca wtrącenia stałe lub pęcherze gazu. W prezentowanych badaniach przedstawiono koncepcję przekształcania pomiarów na obrazy tomograficzne wykorzystującą wiele znanych, homogenicznych metod jednocześnie. Przyjęto założenie, że nie istnieje jedna metoda rozwiązania problemu odwrotnego dla wszystkich możliwych przypadków pomiarowych. W zależności od specyfiki badanego przypadku różne metody generują rekonstrukcje zróżnicowane pod względem dokładności i rozdzielczości. Zaprezentowane badania udowadniają, że proponowane podejście uzasadnia wzrost złożoności obliczeniowej zapewniając wyższą jakość obrazów tomograficznych. (**Hybrydowe uczenie maszynowe w impedancyjnej tomografii elektrycznej**).*

Keywords: electrical tomography; machine learning; industrial tomography.
Słowa kluczowe: tomografia elektryczna; uczenie maszynowe; tomografia przemysłowa.

Introduction

Tomography is a non-invasive imaging technology that allows for visualising the interior of objects [1]. Medical tomography is increasingly being performed using technologies of artificial intelligence. Tomography comes in a variety of forms. Electrical capacitance tomography (ECT) [2], electrical impedance tomography (EIT) [3], computed tomography (CT) [4], radio tomographic imaging (RTI) [5], ultrasonic tomography (UST) [6,7], and others [8–10]. The purpose of this study is to examine the EIT's utility in medical diagnostic applications.

EIT is a subfield of electrical tomography. The EIT works by measuring the voltages between individual electrodes placed on the surface of the object being tested. Therefore, it is critical to specify the background measurements appropriately, i.e., the interior of the test object that is free of inclusions. When inclusions are present, the voltages between the electrode pairs change due to the change in conductivity within the tested object.

Because tomography, particularly EIT, addresses the so-called inverse issue, which is frequently poorly defined (ill-posed), it is challenging to acquire high-resolution and reliable tomographic pictures. Observing the evolution of tomographic methods and algorithms, one can observe a constant effort to build a universal method and produce good results for as many different types of monitored objects as feasible.

A distinctive feature is the simultaneous use of multiple machine learning algorithms, which enables their automatic and instantaneous selection based on two criteria: the measurement case and the tomographic image pixel

Materials and Methods

The prototype hybrid tomograph seen in Figure 1 is capable of connecting up to 32 EIT electrodes. The physical model depicted in Figure 2 is of a tank filled with tap water. In the water, plastic tubes filled with air were plunged. There are 32 electrodes located around the reactor/bucket (see Figure 2). Every second electrode was employed in the presented research for a total of sixteen electrodes.

Fig. 1. The electrical impedance tomography (EIT) device.

Several dozen test measurements were conducted using the thus-prepared physical model. The forward problem was solved using the measurements by altering the parameters of the numerical model based on the finite element approach (FEM). This was accomplished through the usage of the Eidors toolbox [11]. Based on a dense mesh of finite elements, the model created in Eidors accurately provided measurement values. A set of 30000 examples was simulated using this model, including both the data and the accompanying conductivity distributions.

Gaussian noise with a standard deviation of several per cent was applied to the value of each measurement. The triangular finite element mesh, which reflected the reservoir's cross-section, contained 2502 elements.

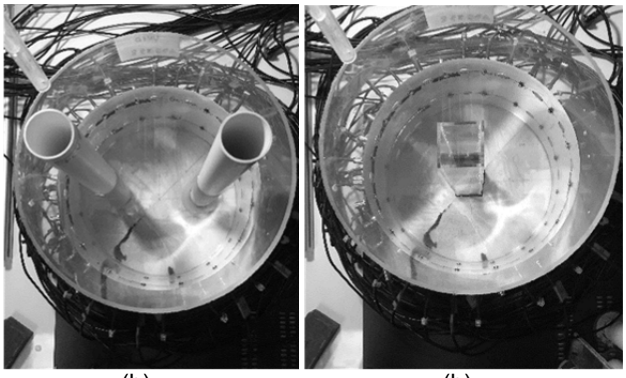

(b) (b)

Fig. 2. Physical model of the reactor with electrodes arranged around: (a) - round phantoms, (b) - square phantom.

Each finished element is a pixel of a tomographic image. Thus, the output image is an illustration of the conductivity distribution of the individual mesh elements.

The Support Vector Machines (SVM) idea presupposes the presence of a decision space that may be partitioned by defining boundaries between items belonging to distinct categories. SVM is a well-known machine learning technique that may be used to solve regression and classification problems. Vladimir Vapnik and his colleagues pioneered this approach in 1992. Support vector models (SVMs) are classified into four categories based on the sort of error function they use: classification type 1 (C-SVM), classification type 2 (ε-SVM), regression type 1 (ε-SVM), regression type 2 (ν-SVM). In SVM regression, we look for the functional dependence of the dependent variable *y* on the set of independent variables *x*. In regression, it is assumed that this relationship is of the deterministic type $f(x)$, with some addition of random noise: $y = f(x) + noise$. The primary objective is thus to determine the shape of the function *f* that will best supply the value of the dependent variable for new cases that the SVM model has not previously "seen". This process is accomplished by training the SVM model system on a set of cases referred to as the learning test. The offered notion implies that each SVM subsystem independently derives the value of a single picture pixel. A complete EIT system has the same number of trained SVMs as the resolution of the output picture, which is $(96 \rightarrow \mathrm{SVM} \rightarrow 1) \times 2502$. The algorithm utilised in these studies maps data into a higher-dimensional space, solving the regression type 2 problem (ν-SVM). The deviation function of the type (1) is reduced to a minimum value:

$$(1) \qquad \frac{1}{2} w^T w - C\left(\nu\varepsilon + \frac{1}{N}\sum_{i=1}^{N}(\xi_i + \xi_i^*)\right)$$

under the following conditions (2, 3, 4):

$$(2) \qquad (w^T \Phi(x_i) + b) - y_i \leq \varepsilon + \xi_i$$
$$(3) \qquad y_i - (w^T \Phi(x_i) + b_i) \leq \varepsilon + \xi_i^*$$
$$(4) \qquad \xi_i, \xi_i^* \geq 0, \;\; i = 1, \ldots, N, \;\; \varepsilon \geq 0$$

where ε, ν are the penalty parameters, C is a constant called the capacity, w is a vector of coefficients, *b* is a constant, and ξ_i, ξ_i^* are the parameters handling overlapping cases. Index *i* numbers the *N* learning cases, x_i are independent variables and y_i are regression patterns. The kernel function transforms the data in the input stream into a new feature space. It should be stressed out that C has a significant effect on the deviation and that its value must be carefully chosen to avoid overfitting the model. Each of the SVM subsystems was trained using 1000 training cases.

In addition to SVMs, a shallow artificial neural network can be used (ANN). The multilayer perceptron was utilised, with ten neurons in the hidden layer. 96 measurements were included in the input vector. The output of the ANN was a real value indicating the conductivity of a single finite element within an image pixel grid. A single network has the structure $(96 \rightarrow 10 \rightarrow 1)$. Like SVM, a comprehensive EIT system based on ANNs is $(96 \rightarrow 10 \rightarrow 1) \times 2502$. Scaled conjugate gradient backpropagation was used to train neural networks. This approach consumes less memory and permits concurrent training on the GPU, which is not achievable with other algorithms, such as the Levenberg-Marquardt method. The hidden layer makes use of the hyperbolic tangent sigmoid function for transfer. The output layer, on the other hand, makes use of the linear transfer function. The training set for ANNs contained 27440 examples. It was separated into training, validation, and test sets in the proportion of 70:15:15. To avoid overfitting, an early halting approach was adopted. After the sixth iteration, which failed to reduce the validation error, the network training process was automatically halted.

This research makes a significant contribution by optimising the "pixel by pixel" reconstruction method by employing a more efficient algorithm (SVM or ANN) to create conductivity values for each pixel. It was anticipated that among all pixels in the EIT image, there are some for which the SVM approach provides superior reconstruction and others for which the ANN method provides superior results. To determine the existence of pixels for which one of the two tested approaches produces superior results, a sample of n=100 randomly selected cases was tested. The resulting image has a resolution of $N_{ij} : i \in [1, 2502], j \in [1, n]$. Let y_{ij} be *i*-th pixel at *j*-th reference (ground-truth) case conductivity, $\hat{y}_{ij}$ be the reconstructed conductivity and $\Delta y_{ij} = y_{ij} - \hat{y}_{ij}$. Let Δy_{ij}^{ANN} be the deviation for *i*-th pixel reconstructed by ANN, and Δy_{ij}^{SVM} be the same for SVM. Let p_{ij} be the binary indicator, such that if $\Delta y_{ij}^{ANN} \leq \Delta y_{ij}^{SVM}$ then $p_{ij} = 1$ otherwise $p_{ij} = 0$. Let $P = \sum_{i=1}^{N}\sum_{j=1}^{n} p_{ij}$ when $N = 2502$ and $n = 100$. Then the percentage predominance $S(P)$ of one of the methods (ANN or SVM) is calculated according to the formula (5)

$$(5) \qquad S(P) = \begin{cases} 2P - 100 & \text{if } 50 \leq P \leq 100 \\ 100 - 2P & \text{otherwise.} \end{cases}$$

Figure 3 shows the Pareto chart. This histogram shows the percentage bins sorted in descending order and a row that shows the cumulative total percentage.

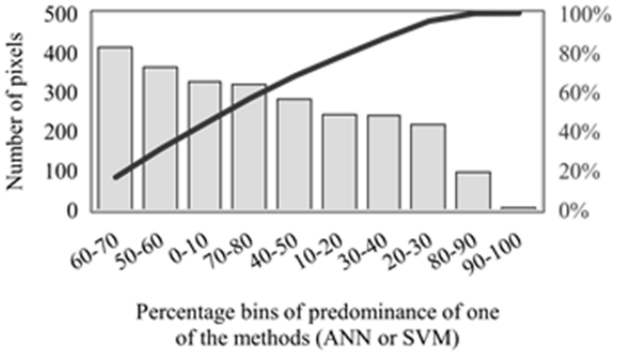

Fig. 3. Pareto chart showing the constant supremacy of one of the two tested methods

The Pareto chart in Figure 3 indicates the most important parts of the dataset as the percentage ranges that demonstrate the effectiveness of the presented concept. It is showing the constant supremacy of one of the two tested methods for the pixels of the tomographic image.

Results

Figure 4 illustrates four test cases that were utilised to validate the presented concept's usefulness. The columns depict the reference image, followed by images generated using the ANN and SVM approaches, and finally, the output image formed by utilising either SVM or ANN selectively based on the pixel. Three of the cases presented in Figure 4 involve reconstructions with inclusions 1 and 2. Unfortunately, visual evaluation of reconstruction is permanently harmed by subjectivism. It can be used in conjunction with the objective assessment based on the MSE, RIE, and ICC indicators. Nonetheless, the reconstructions created using the new hybrid method appear to be the most accurate reference images.

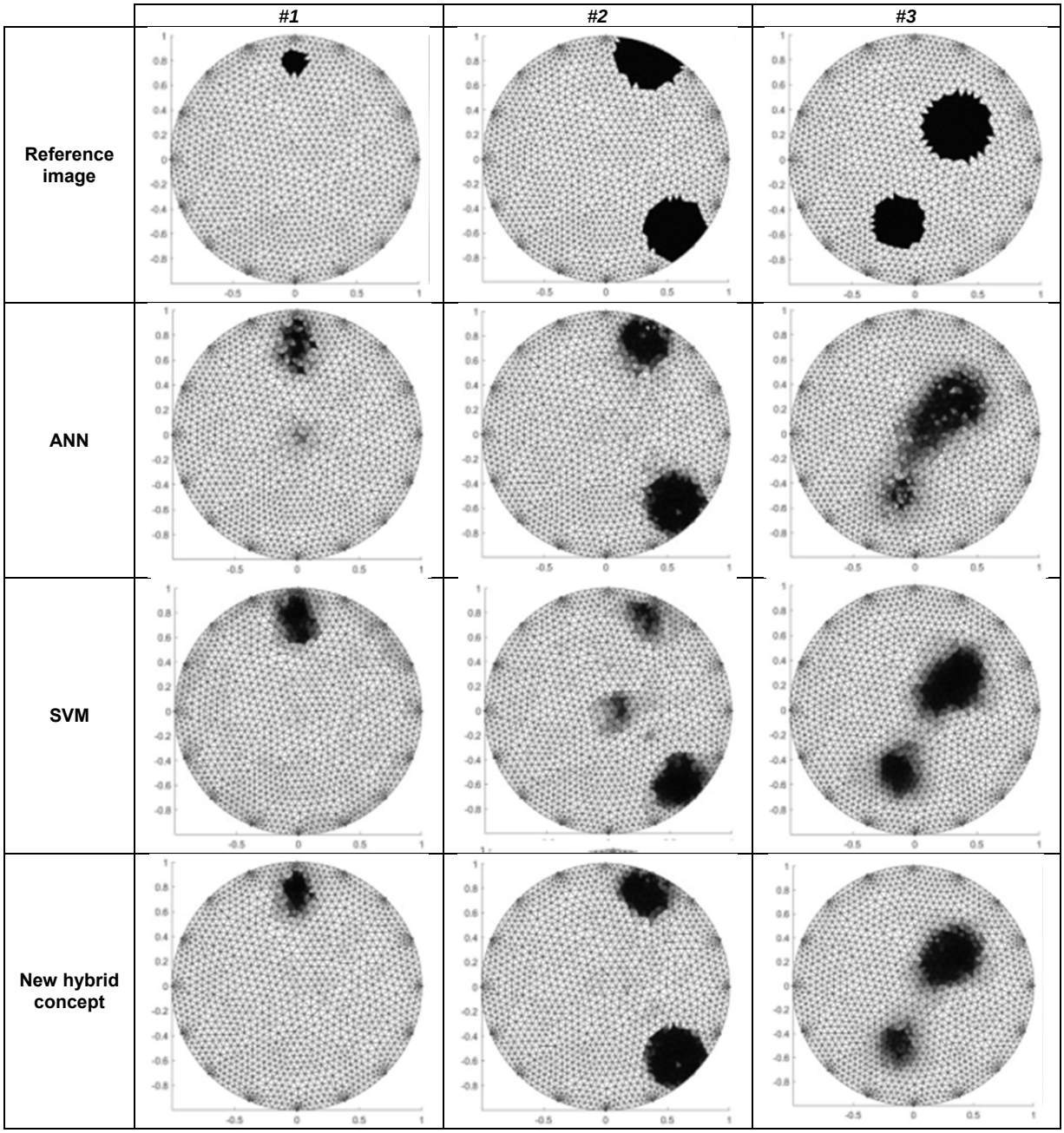

Fig. 4 Test reconstructions for 3 methods: ANN, SVM and selective (ANN or SVM).

Table 1 corresponds to Figure 4, which depicts a comparison of the reconstructions derived using three different metrics. This study aims to compare quantitative indicators that are unique to each of the three investigated methodologies. The first two methods (ANN and SVM) are homogeneous, but the third method is a novel hybrid approach. Each approach was evaluated using three different criteria: MSE, RIE, and ICC. Formula (6) satisfies the mean squared error.

$$\text{MSE} = \frac{\sum_{i=1}^{n} (\Delta y_i)^2}{n} \tag{6}$$

The relative image error is defined by equation (7).

$$\text{RIE} = \frac{\|\Delta y_i\|}{\|\hat{y}_i\|} \tag{7}$$

Table 1. Comparison of image reconstructions

Methods	Evaluation metrics	Investigated cases			Average
		#1	*#2*	*#3*	
Artificial Neural Network	MSE	0.031	0.187	0.238	0.152
	RIE	1.847	1.249	1.537	1.544
	ICC	0.936	0.450	0.753	0.713
Support Vector Machine	MSE	0.031	0.220	0.232	0.161
	RIE	1.842	1.355	1.517	1.571
	ICC	0.848	0.342	0.802	0.664
New hybrid method	MSE	0.029	0.171	0.215	0.138
	RIE	1.792	1.192	1.460	1.481
	ICC	0.947	0.465	0.812	0.741
Is MSE for the new hybrid method the best?		YES	YES	YES	YES
Is RIE for the new hybrid method the best?		YES	YES	YES	YES
Is ICC for the new hybrid method the best?		YES	YES	YES	YES

The image correlation coefficient is often called Pearson's correlation coefficient. It is explained by (8)

$$\text{ICC} = \frac{\sum_{i=1}^{N}(y_i-\bar{y})(\hat{y}_i-\bar{\hat{y}})}{\sqrt{\sum_{i=1}^{N}(y_i-\bar{y})^2 \sum_{i=1}^{n}(\hat{y}_i-\bar{\hat{y}})^2}} \tag{8}$$

where $\bar{y}$ is the mean conductivity of pattern image, and $\bar{\hat{y}}$ is the mean conductivity of reconstructed image. The smaller the MSE and RIE are, the better the quality of the image. ICC have the opposite meaning - the closer to 1, the better correlation between the pattern image and its reconstruction.

When analysing the metrics in Table 1, the best results are obtained by the new method for all three analysed cases. The last column of Table 1 shows the average values of MSE, RIE and ICC indicators for all analysed cases. The last 3 lines of Table 1 show the results of the detailed comparison of the metrics for the ANN and SVM methods with the new hybrid method. In all comparisons, the highest quality of the reconstructive images was achieved thanks to the new concept.

Conclusions

We introduce a novel hybrid pixel-dependent paradigm for EIT systems in this article. The original method presupposed that the quality of reconstructed pixels in a given tomographic image is dependent on the reconstruction technique used. Two machine learning algorithms – SVM and ANN – were trained to validate the initial assumption. Then, pictures were reconstructed using singular ANNs and singular SVMs on a random sample of 100 cases. The reconstruction results for each of the 2502 pixels were compared, and the appropriate approach (ANN or SVM) for each pixel was chosen based on these comparisons. Finally, three test cases were reconstructed using a novel pixel-dependent concept (see Figure 4 and Table 1), and the results were compared to those obtained using a single ANN or SVM. MSE, RIE, and ICC indices demonstrated unequivocally that the new hybrid idea with method selection is more effective than employing a single homogeneous method for all pixels in the tomographic reconstruction.

***Authors**: Tomasz Rymarczyk, Prof. Eng., University of Economics and Innovation, Projektowa 4, Lublin, Poland, E-mail: tomasz.rymarczyk@netrix.com.pl; Grzegorz Kłosowski, Ph.D. Eng., Lublin University of Technology, Nadbystrzycka 38A, Lublin, Poland, E-mail: g.klosowski@pollub.pl; Mirosław Guzik Ph.D., University of Economics and Innovation, Projektowa 4, Lublin, Poland, E-mail: miroslaw.guzik@wsei.lublin.pl; Konrad Niderla, M.Sc. Eng., Lublin University of Economics and Innovation, Projektowa 4, Lublin, Poland, E-mail: konrad.niderla@wsei.lublin.pl; Jerzy Lipski Prof. Eng., Lublin University of Technology, Nadbystrzycka 38A, Lublin, Poland, E-mail: j.lipski@pollub.pl*.

REFERENCES

[1] Rymarczyk, T.; Kłosowski, G. Innovative methods of neural reconstruction for tomographic images in maintenance of tank industrial reactors. Eksploat. i Niezawodn. -- Maint. Reliab. (2019), 21, 261–267.

[2] Rymarczyk T.: New Methods to Determine Moisture Areas by Electrical Impedance Tomography, International Journal of Applied Electromagnetics and Mechanics, 52, 79-87, 2016

[3] Rymarczyk, T.; Kozłowski, E.; Kłosowski, G.; Niderla, K. Logistic Regression for Machine Learning in Process Tomography. Sensors (2019), 19, 3400, doi:10.3390/s19153400.

[4] Babout, L.; Grudzień, K.; Wiącek, J.; Niedostatkiewicz, M.; Karpiński, B.; Szkodo, M. Selection of material for X-ray tomography analysis and DEM simulations: comparison between granular materials of biological and non-biological origins. Granul. Matter (2018), 20, 38, doi:10.1007/s10035-018-0809-y.

[5] Bartusek, K.; Fiala, P.; Mikulka, J. Numerical modeling of magnetic field deformation as related to susceptibility measured with an MR system. Radioengineering (2008), 17, 113–118.

6. Kłosowski, G.; Rymarczyk, T.; Wójcik, D.; Skowron, S.; Cieplak, T.; Adamkiewicz, P. The Use of Time-Frequency Moments as Inputs of LSTM Network for ECG Signal Classification. Electronics (2020), 9, 1452, doi:10.3390/electronics9091452.

[7] Ziolkowski, M.; Gratkowski, S.; Zywica, A.R. Analytical and numerical models of the magnetoacoustic tomography with magnetic induction. COMPEL - Int. J. Comput. Math. Electr. Electron. Eng. (2018), 37, 538–548, doi:10.1108/COMPEL-12-2016-0530.

[8] Sekulska-Nalewajko, J.; Gocławski, J.; Korzeniewska, E. A method for the assessment of textile pilling tendency using optical coherence tomography. Sensors (Switzerland) (2020), 20, 1–19, doi:10.3390/s20133687.

[9] Korzeniewska, E.; Sekulska-Nalewajko, J.; Gocawski, J.; Droż Dż, T.; Kiebasa, P. Analysis of changes in fruit tissue after the pulsed electric field treatment using optical coherence tomography. EPJ Appl. Phys. (2020), 91, 30902, doi:10.1051/epjap/2020200021.

[10] Chen, B.; Abascal, J.; Soleimani, M. Extended Joint Sparsity Reconstruction for Spatial and Temporal ERT Imaging. Sensors (2018), 18, 4014, doi:10.3390/s18114014.

[11] Adler, A.; Lionheart, W.R.B. Uses and abuses of EIDORS: an extensible software base for EIT. Physiol. Meas. (2006), 27, S25–S42, doi:10.1088/0967-3334/27/5/S03.